

Copper Oxide Decorated Carbon Nanofiber Skeleton for Dendrite-Free Lithium-Metal Anodes

Shikun Shao⁺^[a] Hong Liu⁺^[a, b] Chao Wang,^[a] Dabing Li,^[a] Xiaoxue Zhao,^[a] and Li-Zhen Fan^{*[a]}

Lithium metal, possessing a high theoretical capacity, holds great promise as a desirable anode candidate for the next-generation high energy density lithium batteries. However, the practical implementation of lithium metal faces significant challenges, including dendrite growth and volume expansion. Herein, a carbon nanofiber (CNF) three-dimensional (3D) current collector was developed, complemented by the addition of copper oxide nanoparticles to the CNF framework, resulting in the creation of a lithiophilic 3D current collector known as CuO-CNF. Subsequently, a 3D lithium metal composite anode (CuO-CNF-Li) was fabricated through an electrochemical plating process. The utilization of a 3D structure based on carbon

nanofibers provides sufficient space and a stable framework for lithium ion plating, effectively accommodating the substantial volume changes that occur during repetitive Li plating and stripping. The copper oxide nanoparticles loaded onto the CNF serve as active sites for lithium nucleation, facilitating an ordered and uniform plating/stripping process of lithium ions, thereby preventing dendrite formation. Consequently, the CuO-CNF current collector enables dendrite-free Li plating/stripping with an average Coulomb efficiency of up to 99% and a low nucleation overpotential of only 15 mV. Moreover, symmetric cell tests demonstrated an extended lifespan of 2700 h at 2 mA cm⁻² for the CuO-CNF-Li composite anode.

Introduction

The conventional graphite anode in lithium-ion batteries falls short for high-performance portable electronic devices and electric vehicles.^[1–3] Instead, the lithium metal anode has gained attention due to its exceptional characteristics: ultra-high theoretical specific capacity (3861 mAh g⁻¹) and low redox potential (−3.04 V compared to the standard hydrogen electrode).^[4] By coupling the lithium metal anode with various cathode materials, higher energy density can be achieved.^[5,6] Nonetheless, practical applications of the lithium metal anode are confronted with formidable challenges.^[7] Unlike graphite, the lithium metal anode undergoes significant volume fluctuations during lithium plating and stripping, leading to material degradation and shorter battery life. Additionally, dendrite formation is exacerbated by uneven ion plating, which causes decreased Coulomb efficiency, increased battery polarization, and electrode short circuits. These challenges can be addressed by developing a lithiophilic 3D current collector for a composite lithium metal anode. The 3D structure provides a stable

framework that mitigates infinite variations in volume while expanding the surface area and reducing the current density.^[8] Lithiophilic nucleation sites within the 3D skeleton promote uniform lithium ion plating, avoiding dendrite formation.^[9,10]

Early investigations into 3D lithium anodes used metal substrates like copper and nickel as the foundation. These studies involved designing 3D nanostructures on planar metal current collectors, followed by fabricating 3D lithium metal composite anodes through methods like molten lithium injection or electroplating. Li et al. implemented a method wherein planar copper foil was immersed in an alkaline solution, resulting in the generation of Cu(OH)₂ fibers on the copper foil surface through a straightforward chemical oxidation reaction. Subsequent calcination in air yielded a 3D CuO@Cu current collector. The utilization of 3D Cu collectors in cells yielded notable achievements, including high average Coulombic efficiency over 150 cycles (in contrast to 50 cycles for planar Cu) and extended cycle life.^[11] However, the energy density of 3D lithium anodes based on metal material current collectors is significantly diminished due to the often excessive mass of the metal material current collector.^[12–15]

Carbon materials, characterized by their wide availability, low cost, diverse structures, and favorable mechanical properties, can serve various functions in enhancing the performance of lithium metal anodes.^[16–20] Nevertheless, carbon-based materials exhibit Li-phobic properties, resulting in significant barriers for lithium nucleation and uneven distribution of lithium ions, which exacerbate the growth of lithium dendrites on the carbon skeleton. To address this issue and further regulate the plating and stripping behavior of lithium metal on the carrier, functional modifications on the carrier surface become necessary. Various materials, such as ZnO, NiO, CuO, and Co₃O₄, are recognized as lithiophilic materials due to their ability to undergo reversible alloying reactions with lithium.^[21–25]

[a] S. Shao,⁺ H. Liu,⁺ C. Wang, D. Li, X. Zhao, Prof. L.-Z. Fan

Beijing Advanced Innovation Center for Materials Genome Engineering
Beijing Key Laboratory for Advanced Energy Materials and Technologies
University of Science and Technology Beijing, Beijing 100083, China
E-mail: fanlizhen@ustb.edu.cn

[b] H. Liu⁺

State Key Laboratory of New Ceramics and Fine Processing
School of Materials Science and Engineering
Tsinghua University, Beijing 100084, China

[+] These authors contributed equally to this work

Supporting information for this article is available on the WWW under
<https://doi.org/10.1002/batt.202300303>

An invited contribution to a Special Collection on Young Scientists in Battery Research

These lithophilic materials can be adorned onto the surface of the conductive skeleton, serving as guides for the uniform deposition of lithium. Moreover, their favorable lithium affinity ensures the initial uniform deposition of lithium on the material's surface.

In this study, we fabricate a lithophilic 3D current collector by constructing a 3D carbon nanofiber (CNF) skeleton through electrospinning and heat treatment. Nano-sized copper oxide particles are loaded onto the CNF using two distinct methods, resulting in the formation of CuO-CNF and CuO@CNF, as illustrated in Figure 1(a). Subsequently, a long cycle life, dendrite-free 3D lithium metal composite anode (CuO-CNF–Li) is prepared via electrochemical plating. The 3D structure and large specific surface area of the CNF provide ample space and a stable framework for lithium ion plating, effectively addressing the significant volume changes associated with repeated plating and stripping processes. The incorporation of nano-sized copper oxide particles on the CNF serves as active sites with low nucleation polarization, promoting the formation of uniform lithium metal nuclei and facilitating orderly lithium ion plating, thus preventing dendrite formation. The CuO-CNF current collector demonstrates excellent cycling stability, maintaining stable performance for 300 cycles in half-battery charge-discharge tests, with an impressive average Coulomb efficiency (CE) of 99%. Compared to traditional copper current collectors, the CuO-CNF exhibits lower nucleation overpotential for lithium. Moreover, the CuO-CNF–Li composite anode exhibits a

prolonged lifespan of 2700 h in symmetric cell tests conducted at a current density of 2 mA cm^{-2} .

Results and Discussion

The 3D carbon nanofibers, fabricated through electrospinning and heat treatment, exhibit excellent electron collection properties. Distinct preparation methods are employed for CuO@CNF and CuO-CNF, resulting in different distributions of copper oxide nanoparticles on the carbon fiber. In the case of CuO@CNF, the process involves first preparing the carbon nanofiber current collector and subsequently immersing it in a solution of copper nitrate, facilitating the adsorption of copper nitrate particles onto the carbon fiber skeleton. Upon heating, the copper nitrate undergoes a decomposition reaction, leading to the formation of copper oxide. The well-crystallized phase of the in-situ generated CuO is confirmed by the X-ray diffraction pattern of CuO@CNF, as illustrated in Figure 1b. Conversely, CuO-CNF is prepared by uniformly mixing copper oxide nanoparticles with PAN to form a spinning solution, which is then directly subjected to electrospinning.^[26] Figure 2(a) depicts a scanning electron microscopy (SEM) image of the carbon nanofiber (CNF) without immersion in a copper nitrate solution. The carbon fiber surface appears smooth, uniform, overlapping, and randomly oriented. SEM image (Figure 2b) and energy-dispersive X-ray spectroscopy (EDS) images (Figure 2c) of

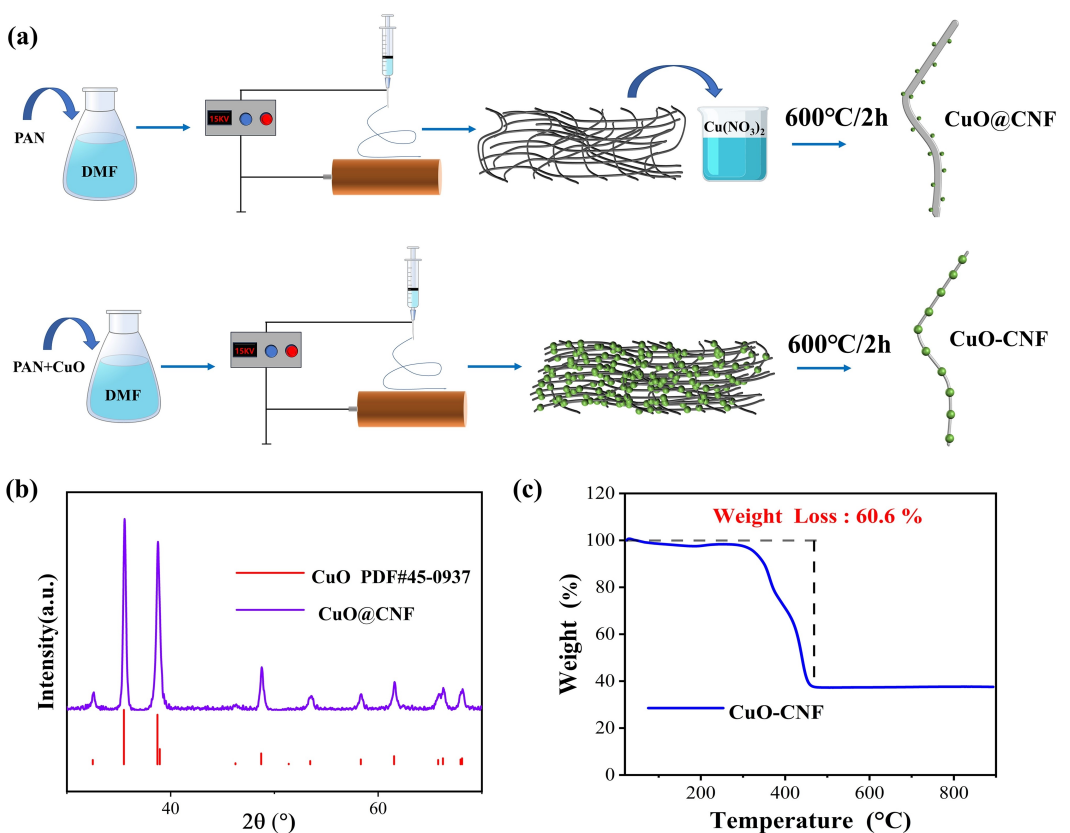


Figure 1. a) Schematic diagram of the preparation process of CuO@CNF and CuO-CNF. b) XRD patterns of the CuO@CNF. c) TGA of CuO-CNF in air atmospheres.

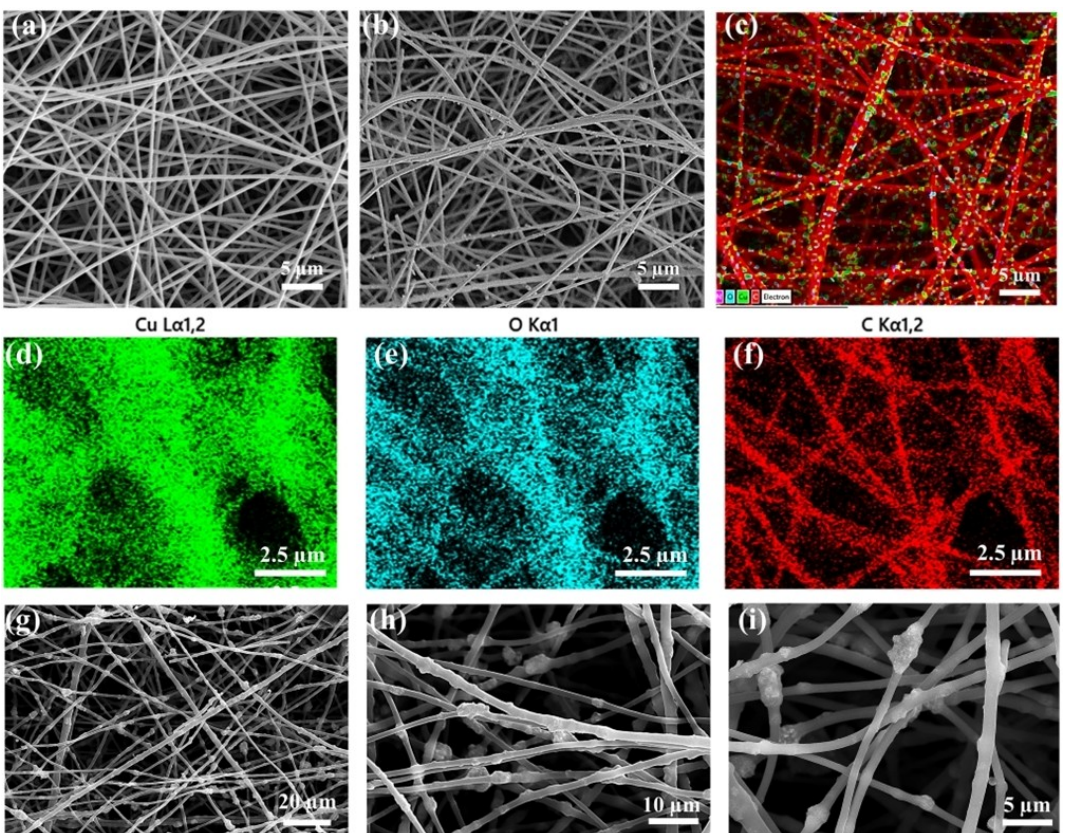


Figure 2. SEM images of the surface of a) CNF and b) CuO@CNF. c) EDS spectra of CuO@CNF. d, e and f) are the corresponding elemental mapping of Cu, O and C, respectively. g, h and i) are SEM images under the conditions of CuO-CNF amplification at 2000 times, 5000 times and 10000 times, respectively.

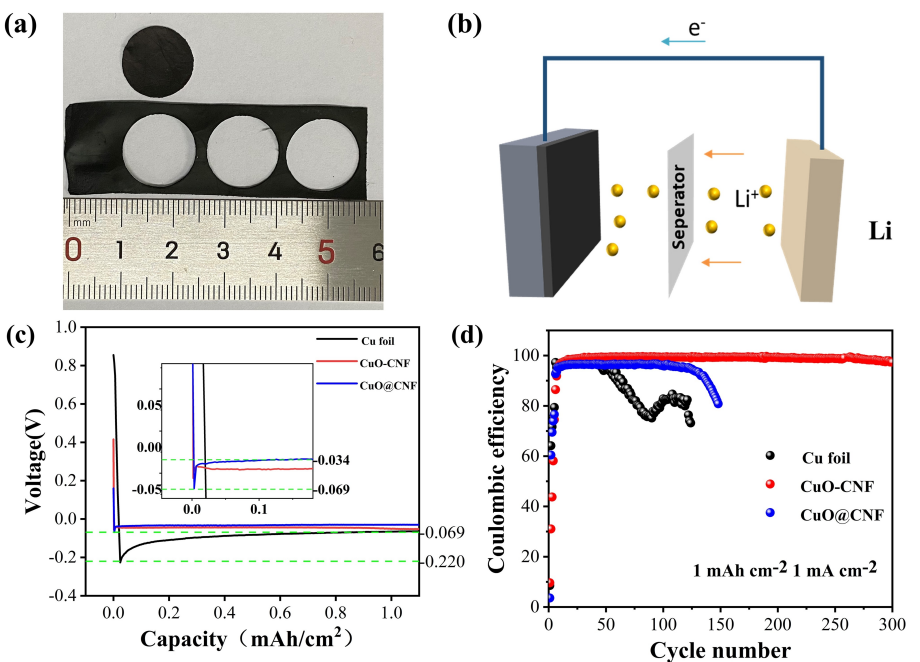


Figure 3. a) Optical images of CuO@CNF and CuO-CNF. b) Schematic diagram of half-cell test. c) Comparison of overpotential of Li nucleation on Cu foil, CuO@CNF, and CuO-CNF. d) CE test of Cu || Li, CuO@CNF || Li and CuO-CNF || Li at a current density of 1 mA cm^{-2} and plating capacity of 1 mAh cm^{-2} .

CuO@CNF illustrate the uniform distribution of copper oxide on the carbon fiber surface. Elemental mapping of Cu, O, and C are

displayed in Figures 2(d–f) accordingly. Unlike Cu@CNF, copper oxide in CuO-CNF is inserted into the carbon fibers. SEM images

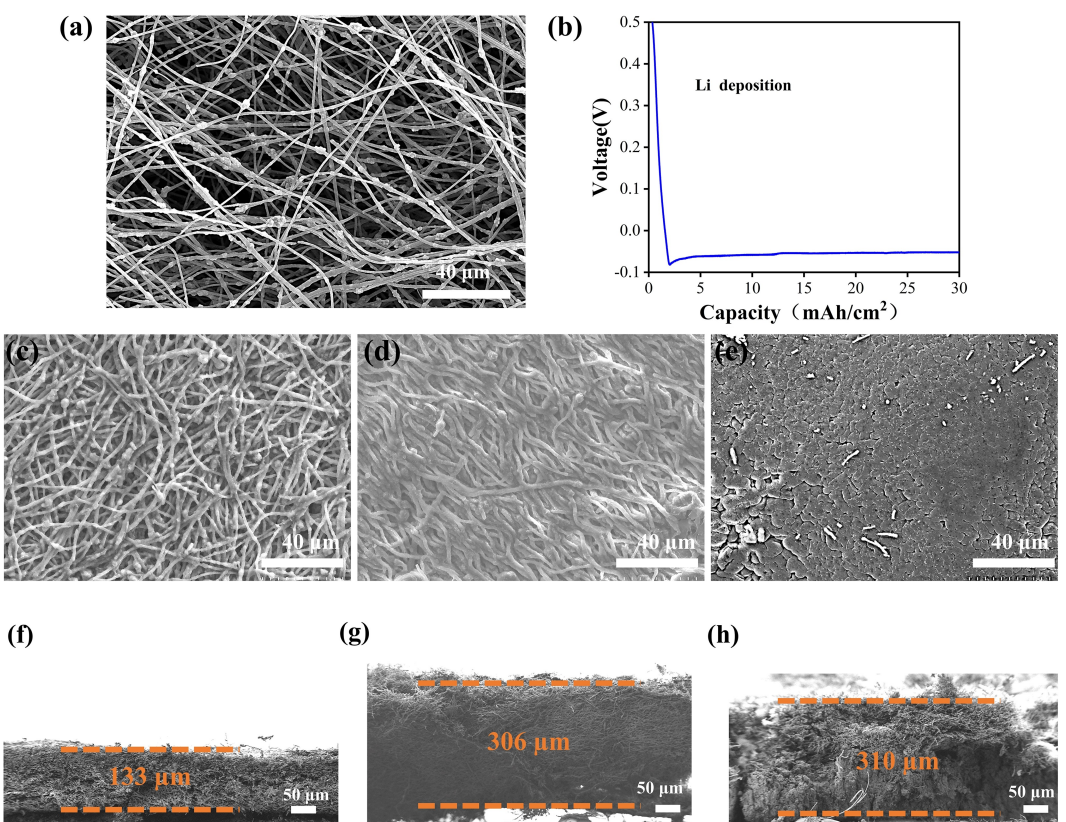


Figure 4. a) SEM images of the surface of CuO-CNF. b) The capacity-voltage curve of Li deposition on CuO-CNF. c, d and e) are the planar SEM of CuO-CNF at Li plating capacity of 10, 20 and 30 mAh cm^{-2} , respectively. f, g and h) are the cross-section SEM of CuO-CNF at Li plating capacity of 10, 20 and 30 mAh cm^{-2} , respectively.

at magnifications of 2000, 5000, and 10000 times for CuO-CNF are shown in Figures 2(g-i). The thermogravimetric analysis curve of CNF-CuO under an air atmosphere is presented in Figure 1(c). Heating CNF-CuO from room temperature to 900 °C results in a mass loss of 60.6%, indicating a carbon-to-copper oxide mass ratio of approximately 3:2. The surface properties of the substrate significantly influence the nucleation behavior of lithium.^[27–31] Lithiophilic materials, including CuO, NiO, ZnO, and Co₃O₄, are known to undergo reversible alloying reactions with lithium.^[32–35] By introducing lithiophilic metal oxides onto the surface of the conductive skeleton, a multitude of nucleation sites can be provided, reducing nucleation polarization and promoting the uniform plating of lithium ions.^[36,37]

To assess the lithiophilicity and reversibility of Li plating/stripping processes, we fabricated disk-shaped working electrodes with a 14.00 mm diameter using the as-prepared CuO@CNF, CuO-CNF, and Cu foil, as shown in Figure 3a and 3b. Li foil served as the counter electrode. The lithiophilicity of the material, indicating the propensity for lithium-ion deposition, is determined by the nucleation overpotential. A lower nucleation overpotential indicates better lithiophilicity. The nucleation overpotential is defined as the difference between the sharp tip voltage and the later stable mass transfer-controlled overpotential, which evaluates lithiophilicity.^[38] Figure 3(c) demonstrates that the nucleation overpotential of Li on Cu foil is approximately 150 mV, whereas on CuO@CNF, it reduces to

35 mV, and on CuO-CNF, it reaches only about 15 mV. To investigate the reversibility of Li plating/stripping, cyclic tests were conducted at a current density of 1 mA cm^{-2} and a plating capacity of 1 mAh cm^{-2} . As depicted in Figure 3(d), the Cu || Li system maintains stability for the initial 50 cycles; however, beyond that, the cell performance deteriorates rapidly due to the uneven deposition of lithium on the Cu foil, leading to the formation of lithium dendrites. In contrast, CuO@CNF || Li exhibits stable cycling performance with a 97% Coulombic efficiency (CE) over 100 cycles, followed by a gradual decrease in CE. Notably, CuO-CNF || Li demonstrates stable charge-discharge cycles for 300 cycles, achieving a CE as high as 99%. Hence, the introduction of lithiophilic functional group CuO into 3D carbon nanofibers with a high specific surface area enhances the reversibility of the Li plating/stripping cycle, thereby extending battery life. Particularly, the CuO-CNF composite, where CuO is distributed on CNF in an inserted manner, achieves a highly stable dendrite-free charge-discharge cycle.

To investigate the Li plating behavior of CuO-CNF, a two-electrode cell configuration with CR2032 coin cells was employed, using CuO-CNF as the working electrode and lithium foil as the counter/reference electrode. The surface of CuO-CNF was examined through SEM imaging, as shown in Figure 4(a). Additionally, the capacity-voltage curve of Li deposition on CuO-CNF during discharge was presented in Figure 4(b). When

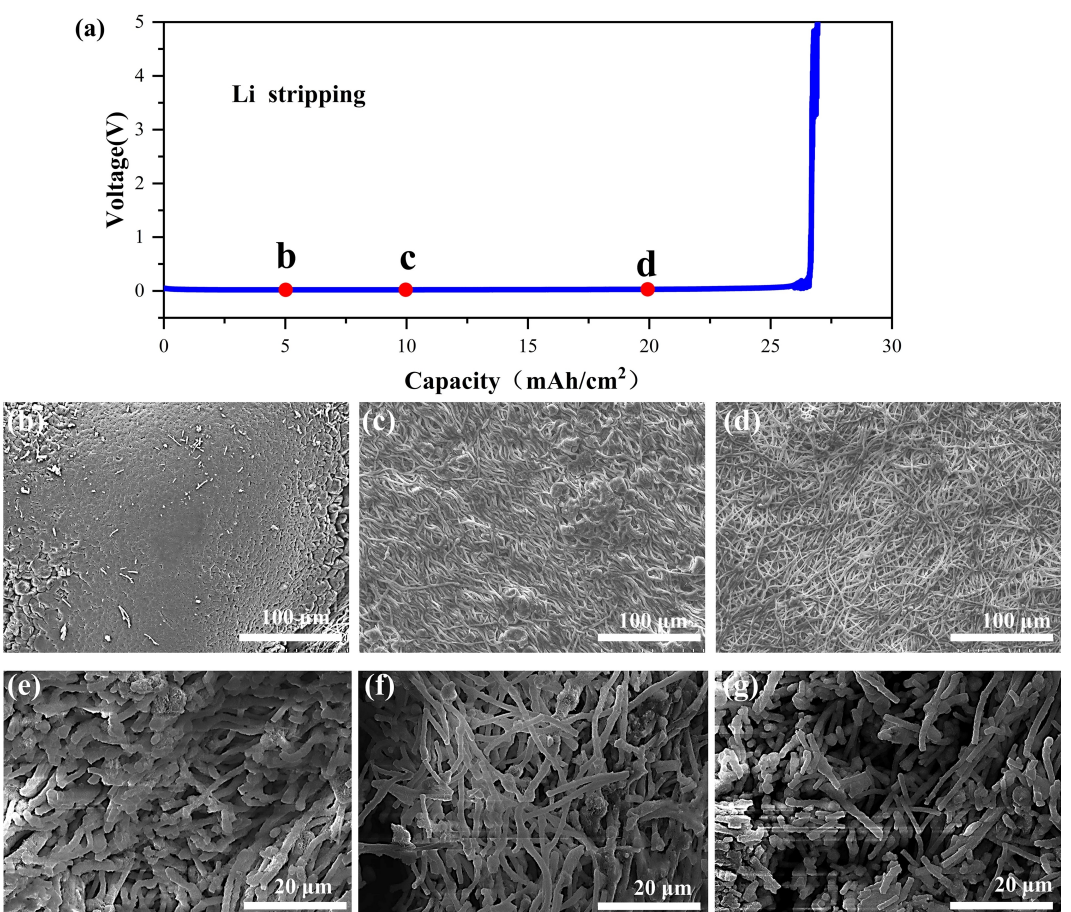


Figure 5. a) The capacity-voltage curve of Li when stripped from CuO-CNF. b, c and d) correspond to the plane SEM of points b, c and d in (a) respectively. e, f and g) correspond to the SEM of the cross sections of points b, c and d in (a), respectively.

the voltage drops below 0 V, Li nucleation initiates on CuO-CNF, and during the process of lithium deposition, the predominant electrochemical reaction occurs between CuO and Li, as expressed by $2\text{Li} + \text{CuO} \rightarrow \text{Cu} + \text{Li}_2\text{O}$. The formation of Li_2O results in an irreversible inactive phase.^[39,40] In subsequent cycles, a reversible alloying reaction takes place between Li and Cu, as depicted by $\text{Li} + \text{Cu} \leftrightarrow \text{LiCu}$.^[41]

When the Li plating capacity reached 10 mAh cm⁻², the carbon fibers exhibited uniform coarsening while retaining their fibrous morphology (Figure 4c), with no observable lithium dendrites. At a plating capacity of 20 mAh cm⁻² (Figure 4d), CuO-CNF-Li displayed a smooth strip structure. Further increasing the plating capacity to 30 mAh cm⁻² resulted in a transformation of CuO-CNF-Li morphology into a smooth, massive structure, yet no Li dendrites were observed (Figure 4e). Figure S3 provides a partial magnification of Figure 4(e), revealing an even distribution of lithium on the surface of the massive fibers. This indicates that CuO-modified CNF, where CuO is inserted within CNF, effectively regulates Li ion deposition and suppresses dendrite formation. Cross-sectional morphologies of CuO-CNF-Li at Li plating capacities of 10 mAh cm⁻², 20 mAh cm⁻², and 30 mAh cm⁻² are respectively illustrated in Figure 4(f-h). It is evident that the thickness of the CuO-CNF-Li cross-section gradually increases with higher Li

plating capacity. This is attributed to the excellent flexibility of CNF, enabling it to accommodate the volume changes associated with lithium metal. Moreover, CNF possesses ample internal space, effectively confining Li within its structure. A CR2032 coin cell was assembled with a CuO-CNF electrode pre-deposited with approximately 30 mAh cm⁻² of Li to observe the Li stripping process. The capacity-voltage curve during Li stripping from CuO-CNF-Li is presented in Figure 5(a). Figure 5(b-d) respectively corresponds to points b, c, and d in Figure 5(a). Notably, as the Li stripping capacity increases, the nanofiber structure re-emerges. The SEM images in Figure 5(e-g) depict the cross-section of CuO-CNF-Li corresponding to the progressive increase in Li stripping capacity. It is evident that the strip structure gradually transforms back into a fibrous shape.

The remarkable ability of CuO-CNF to effectively control Li plating and stripping can be attributed to the synergistic effect of its high specific surface area structure and the incorporation of lithophilic CuO nanoparticles. The 3D carbon fiber skeleton, characterized by its high specific surface area, plays a pivotal role in reducing local current density and facilitating uniform Li metal deposition. Simultaneously, the lithophilic copper oxide nanoparticles act as nucleation sites, guiding the distribution of crystal nuclei. As a result, CuO-CNF-Li exhibits exceptional

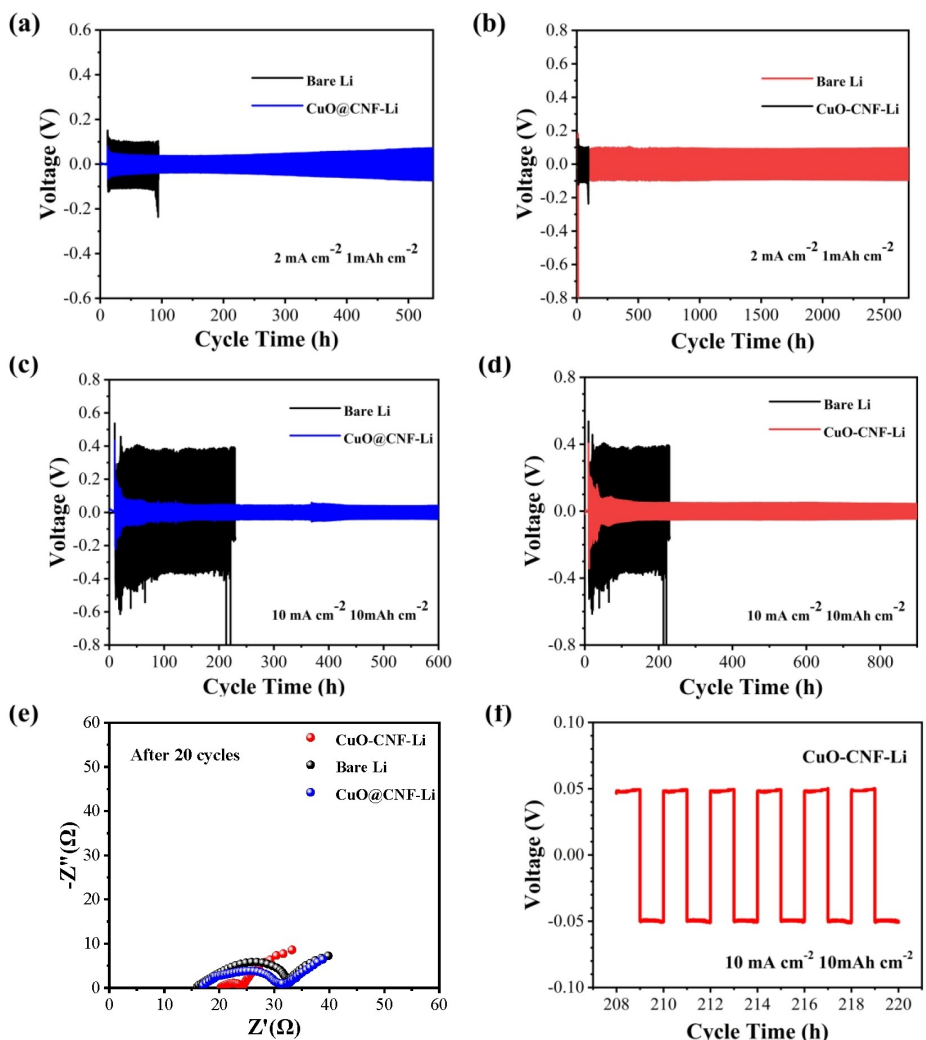


Figure 6. a, b) Galvanostatic cycling voltage profiles of bare Li, CuO@CNF–Li, and CuO-CNF–Li anodes in symmetric coin cells at 2 mA cm^{-2} with a capacity of 1 mAh cm^{-2} . c, d) Galvanostatic cycling voltage profiles of bare Li, CuO@CNF–Li, and CuO-CNF–Li anodes in symmetric coin cells at 10 mA cm^{-2} with a capacity of 10 mAh cm^{-2} . e) The electrochemical impedance spectroscopy of symmetric cells was performed before and after 20 cycles. f) CuO-CNF–Li | CuO-CNF–Li partial figure of its plating/stripping at a current density of 10 mA cm^{-2} .

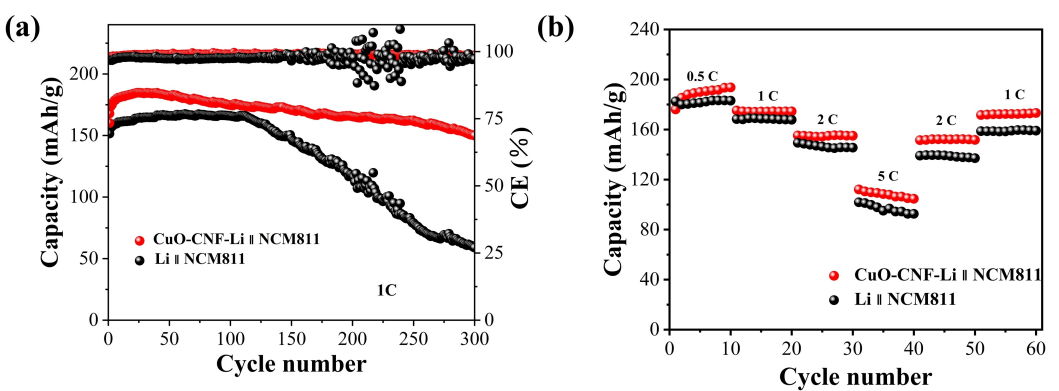


Figure 7. a) Cycling performance of full cell at 1 C. b) Rate performance of full cell.

stability in charge-discharge cycles, devoid of dendrite formation, ensuring reliable and long-lasting performance.

To assess the sustainability and reversibility of the CuO-CNF host for Li metal composite anodes, we pre-deposited 10 mAh cm^{-2} of Li onto CuO@CNF and CuO-CNF, yielding 3D

lithium metal composite anodes, namely CuO@CNF–Li and CuO-CNF–Li, for symmetric cell and full cell testing. As depicted in Figure 6(a and b), the symmetrical cell consisting of bare Li exhibits a voltage drop after 100 h of continuous charge-discharge cycling at a constant current (2 mA cm^{-2}), indicating an internal short circuit. In contrast, under the same current density, CuO@CNF–Li | CuO@CNF–Li demonstrates a prolonged cycling stability of 500 h without encountering a short circuit, while CuO-CNF–Li | CuO-CNF–Li exhibits remarkable ultra-long cycle stability of 2700 h. Even at a high current density of 10 mA cm^{-2} , CuO@CNF–Li | CuO@CNF–Li maintains stable cycling for 600 h and CuO-CNF–Li | CuO-CNF–Li achieves a stable cycle for approximately 900 h, as shown in Figure 6(c and d). Electrochemical impedance spectroscopy measurements of symmetric cells conducted before and after 20 cycles reveal that the interfacial transfer impedance of the two 3D Li metal composite anodes is lower than that of bare Li, as depicted in Figure 6(e). Figure 6(f) displays a partial view of the plating/stripping process of CuO-CNF–Li | CuO-CNF–Li at a current density of 10 mA cm^{-2} , highlighting its stable voltage polarization at approximately 50 mV.

The electrochemical characterization of half cells and symmetrical cells reveals the superior lithiophilicity and exceptional cycle stability of CuO-CNF–Li in comparison to CuO@CNF–Li. This compelling observation motivated us to employ CuO-CNF–Li in conjunction with the commercially available NCM811 cathode material to construct a full cell for the practical assessment. Encouragingly, as illustrated in Figure 7(a), the CuO-CNF–Li | NCM811 configuration exhibits an impressive capacity retention rate of up to 94% after 200 cycles, further demonstrating 85% retention after 300 cycles. Remarkably, Figure 7b showcases the enhanced specific capacity delivered by CuO-CNF–Li | NCM811, with values of 174, 155, and 108 mAh g^{-1} achieved at 1, 2, and 5 C rates, respectively. In contrast, the Li | NCM811 configuration achieves lower specific capacities of 168, 145, and 95 mAh g^{-1} under the same conditions. It is noteworthy that CuO-CNF–Li has a higher discharge capacity than CuO@CNF–Li during the initial discharge in the rate performance test of full cell, which is mainly due to the irreversible reaction experienced by CuO-CNF–Li ($2\text{Li} + \text{CuO} \rightarrow \text{Cu} + \text{Li}_2\text{O}$) during the early lithium deposition process. These remarkable results highlight the substantial advantages of utilizing CuO-CNF–Li as a highly efficient anode material in conjunction with NCM811 for advanced battery applications.

Conclusions

In summary, we have successfully fabricated a lithiophilic 3D current collector (CuO-CNF) to achieve a dendrite-free lithium metal composite anode. The implementation of a 3D carbon fiber skeleton effectively mitigates volume changes during lithium plating and stripping processes, thereby reducing local current density. Furthermore, the lithiophilic nature of the CuO nanoparticles imparts a negligible polarization effect and an ultralow nucleation overpotential. The synergistic interplay between these two components enables effective regulation of

lithium nucleation and growth behavior on the CuO-CNF electrode. Consequently, the CuO-CNF composite exhibits outstanding cycling stability in a half-cell configuration, attaining a high Coulombic efficiency (CE) of 99% throughout multiple cycles. Moreover, even at an ultra-high current density of 10 mA cm^{-2} , the CuO-CNF–Li symmetric cell demonstrates an extraordinarily long cycle life of 2700 h. Notably, when integrated into full cells alongside NCM811 cathodes, the CuO-CNF–Li anode exhibits superior rate capability and maintains a stable cycle life. These impressive results establish the potential of our developed 3D lithium composite anodes to significantly enhance the practicality of lithium metal batteries.

Acknowledgements

Financial supports from the National Key Research and Development Program of China (SQ2022YFB3800005) and National Natural Scientific Foundation of China (U21A2080) and the Beijing Natural Science Foundation (Z200011) are gratefully acknowledged.

Conflict of Interests

The authors declare no conflict of interest.

Data Availability Statement

The data that support the findings of this study are available from the corresponding author upon reasonable request.

Keywords: lithium metal anode • carbon nanofibers • lithium dendrite • CuO nanoparticle

- [1] R. Chen, Q. Li, X. Yu, L. Chen, H. Li, *Chem. Rev.* **2020**, *120*, 6820–6877.
- [2] W. Xu, J. Wang, F. Ding, X. Chen, E. Nasybulin, Y. Zhang, J.-G. Zhang, *Energy Environ. Sci.* **2014**, *7*, 513–537.
- [3] D. Lin, Y. Liu, Y. Cui, *Nat. Nanotechnol.* **2017**, *12*, 194–206.
- [4] X.-B. Cheng, R. Zhang, C.-Z. Zhao, Q. Zhang, *Chem. Rev.* **2017**, *117*, 10403–10473.
- [5] S. Huang, W. Zhang, H. Ming, G. Cao, L.-Z. Fan, H. Zhang, *Nano Lett.* **2019**, *19*, 1832–1837.
- [6] K. Yan, B. Sun, P. Munroe, G. Wang, *Energy Storage Mater.* **2018**, *11*, 127–133.
- [7] W. Ren, Y. Zheng, Z. Cui, Y. Tao, B. Li, W. Wang, *Energy Storage Mater.* **2021**, *35*, 157–168.
- [8] H. Yuan, X. Ding, T. Liu, J. Nai, Y. Wang, Y. Liu, C. Liu, X. Tao, *Mater. Today* **2022**, *53*, 173–196.
- [9] S. Park, H. Jin, Y. S. Yun, *Adv. Mater.* **2020**, *32*, 2002193.
- [10] Y. Cheng, J. Chen, Y. Chen, X. Ke, J. Li, Y. Yang, Z. Shi, *Energy Storage Mater.* **2021**, *38*, 276–298.
- [11] S. Li, Q. He, K. Chen, S. Huang, F. Wu, G. Wang, W. Sun, S. Fu, X. Feng, Y. Zhou, Z. Jiao, *J. Electrochem. Soc.* **2021**, *168*, 070502.
- [12] L.-H. Kong, P.-Y. Zhang, *Langmuir* **2021**, *37*, 759–768.
- [13] Q. Li, S. Zhu, Y. Lu, *Adv. Funct. Mater.* **2017**, *27*, 1606422.
- [14] T. Gao, D. Xu, Z. Yu, Z.-H. Huang, J. Cheng, Y. Yang, *J. Alloys Compd.* **2021**, *865*, 158908.
- [15] Y. Liu, S. Zhang, X. Qin, F. Kang, G. Chen, B. Li, *Nano Lett.* **2019**, *19*, 4601–4607.

- [16] Z. Y. Wang, Z. X. Lu, W. Guo, Q. Luo, Y. H. Yin, X. B. Liu, Y. S. Li, B. Y. Xia, Z. P. Wu, *Adv. Mater.* **2021**, *33*, 2006702.
- [17] Y. Deng, H. Lu, Y. Cao, B. Xu, Q. Hong, W. Cai, W. Yang, *J. Power Sources* **2019**, *412*, 170–179.
- [18] D. Lin, Y. Liu, Z. Liang, H.-W. Lee, J. Sun, H. Wang, K. Yan, J. Xie, Y. Cui, *Nat. Nanotechnol.* **2016**, *11*, 626–632.
- [19] L. Wang, H. Wang, M. Cheng, Y. Hong, M. Li, H. Su, J. Sun, J. Wang, Y. Xu, *ACS Appl. Energ. Mater.* **2021**, *4*, 6245–6252.
- [20] Q. Lu, Y. Jie, X. Meng, A. Omar, D. Mikhailova, R. Cao, S. Jiao, Y. Lu, Y. Xu, *Carbon Energy* **2021**, *3*, 957–975.
- [21] R. Pathak, K. Chen, F. Wu, A. U. Mane, R. V. Bugga, J. W. Elam, Q. Qiao, Y. Zhou, *Energy Storage Mater.* **2021**, *41*, 448–465.
- [22] Q. Wang, B. Liu, Y. Shen, J. Wu, Z. Zhao, C. Zhong, W. Hu, *Adv. Sci.* **2021**, *8*, 2101111.
- [23] S. Xu, D. W. McOwen, C. Wang, L. Zhang, W. Luo, C. Chen, Y. Li, Y. Gong, J. Dai, Y. Kuang, C. Yang, T. R. Hamann, E. D. Wachsman, L. Hu, *Nano Lett.* **2018**, *18*, 3926–3933.
- [24] H. Liu, Y. Liang, C. Wang, D. Li, X. Yan, C.-W. Nan, L.-Z. Fan, *Adv. Mater.* **2022**, 2206013.
- [25] X. Li, W. Chen, Q. Qian, H. Huang, Y. Chen, Z. Wang, Q. Chen, J. Yang, J. Li, Y. Mai, *Adv. Energy Mater.* **2021**, *11*, 2000845.
- [26] N. Chakraborty, J. Banerjee, P. Chakraborty, A. Banerjee, S. Chanda, K. Ray, K. Acharya, J. Sarkar, *Green Chem. Lett. Rev.* **2022**, *15*, 187–215.
- [27] Y. Liu, J. Sun, X. Hu, Y. Li, H. Du, K. Wang, Z. Du, X. Gong, W. Ai, W. Huang, *Nano Energy* **2022**, *94*, 106883.
- [28] X. Wu, W. Zhang, N. Wu, S. Pang, Y. Ding, G. He, *Adv. Energy Mater.* **2021**, *11*, 2003082.
- [29] X. Chen, B. Zhao, C. Yan, Q. Zhang, *Adv. Mater.* **2021**, *33*, 2004128.
- [30] R. Zhang, X. Shen, X.-B. Cheng, Q. Zhang, *Energy Storage Mater.* **2019**, *23*, 556–565.
- [31] Z. Zeng, W. Li, X. Chen, X. Liu, *Adv. Funct. Mater.* **2020**, *30*, 2004650.
- [32] X.-Y. Yue, J. Bao, Q.-Q. Qiu, R.-J. Luo, Q.-C. Wang, X.-J. Wu, Y.-N. Zhou, *Chem. Eng. J.* **2020**, *391*, 123516.
- [33] G. Park, H. Kang, J.-W. Lee, *J. Alloys Compd.* **2019**, *790*, 847–852.
- [34] C. Zhao, X. Yao, H. Yang, X. Jiao, L. Wang, *Compos. Commun.* **2021**, *26*, 100789.
- [35] Y. Fu, L. Li, S. Ye, P. Yang, P. Liao, X. Ren, C. He, Q. Zhang, J. Liu, *J. Mater. Chem. A* **2021**, *9*, 453–462.
- [36] F. Zhao, X. Zhou, W. Deng, Z. Liu, *Nano Energy* **2019**, *62*, 55–63.
- [37] A. Abdul Razzaq, X. Yuan, Y. Chen, J. Hu, Q. Mu, Y. Ma, X. Zhao, L. Miao, J.-H. Ahn, Y. Peng, Z. Deng, *J. Mater. Chem. A* **2020**, *8*, 1298–1306.
- [38] S. Huang, H. Zhang, L.-Z. Fan, *ACS Appl. Mater. Interfaces* **2022**, *14*, 17539–17546.
- [39] R. Zhu, H. Yang, L. Fadillah, Z. Xiong, D. Kowalski, C. Zhu, S. Kitano, Y. Aoki, H. Habazaki, *J. Mater. Chem. A* **2021**, *9*, 13332–13343.
- [40] M. Lei, Z. You, L. Ren, X. Liu, J.-G. Wang, *J. Power Sources* **2020**, *463*, 228191.
- [41] S. Huang, L. Chen, T. Wang, J. Hu, Q. Zhang, H. Zhang, C. Nan, L.-Z. Fan, *Nano Lett.* **2021**, *21*, 791–797.

Manuscript received: July 10, 2023

Revised manuscript received: August 5, 2023

Accepted manuscript online: August 10, 2023

Version of record online: September 6, 2023